Bioorganic Chemistry 87 (2019) 218–226

Contents lists available at ScienceDirect

Bioorganic Chemistry

journal homepage: www.elsevier.com/locate/bioorg

Investigation of new quinoline derivatives as promising inhibitors of NTPDases: Synthesis, SAR analysis and molecular docking studies

Komal Hayat[a], Saira Afzal[b], Altaf Saeed[a], Amna Murtaza[a], Shafiq Ur Rahman[b], Khalid Mohammed Khan[c,d], Aamer Saeed[a], Sumera Zaib[b], Joanna Lecka[e,f], Jean Sévigny[e,f], Jamshed Iqbal[b,*], Abbas Hassan[a,*]

[a] Department of Chemistry, Quaid-i-Azam University, Islamabad 45320, Pakistan
[b] Centre for Advanced Drug Research, COMSATS University Islamabad, Abbottabad Campus, Abbottabad 22060, Pakistan
[c] H.E. J. Research Institute of Chemistry, International Center for Chemical and Biological Sciences, University of Karachi, Karachi 75720 Pakistan
[d] Department of Clinical Pharmacy, Institute for Research and Medical Consultations (IRMC), Imam Abdulrahman Bin Faisal University, P.O. Box 31441, Dammam, Saudi Arabia
[e] Département de microbiologie-infectiologie et d'immunologie, Faculté de Médecine, Université Laval, Québec, QC G1V 0A6, Canada
[f] Centre de Recherche du CHU de Québec – Université Laval, Québec, QC G1V 4G2, Canada

ARTICLE INFO

Keywords:
Quinoline synthesis
Iodine catalysis
NTPDase inhibitors
Structure-activity relationship

ABSTRACT

Nucleoside triphosphate diphosphohydrolases (NTPDases), an important class of ectonucleotidases, are responsible for the sequential hydrolysis of extracellular nucleotides. However, over-expression of NTPDases has been linked with various pathological diseases *e.g.* cancer. Thus, to treat these diseases, the inhibitors of this class of enzyme are of interest. The significance of this class of enzyme encouraged us to synthesize a new class of quinoline derivatives with the aim to find selective and potent inhibitors of NTPDases. Therefore, a mild and efficient synthetic route was established for the synthesis of quinoline derivatives. The reaction was catalyzed by molecular iodine to afford the substituted quinoline derivatives. All the synthetic derivatives (**3a-3w**) were evaluated for their potential to inhibit the *h*-NTPDase1, 2, 3 and 8. Most of the compounds were identified as dual inhibitors of *h*-NTPDase1 and 8 with lower effects on *h*-NTPDase2 and 3. Two compounds *i.e.* **3f** and **3t** were identified as selective inhibitor of *h*-NTPDase1 whereas the compound **3s** inhibited the *h*-NTPDase8 selectively. Moreover, the compounds **3p** (IC_{50} = 0.23 ± 0.01 μM), **3j** (IC_{50} = 21.0 ± 0.03 μM) **3d** (IC_{50} = 5.38 ± 0.21 μM) and **3c** (IC_{50} = 1.13 ± 0.04 μM) were found to be the most potent inhibitors of *h*-NTPDase1, 2, 3 and 8, respectively. To determine the binding interaction, molecular docking studies were also carried out.

1. Introduction

In the past decades, ATP was strictly thought to be a part of intracellular realm where it had been associated with energy transactions and cell metabolism. However, it is now well established that ATP and its metabolites also act as extracellular cell signaling molecules and elicit multiple biological effects including neurotransmission, immune responses, wound healing, cell growth and proliferation, bone formation and resorption [1]. The extracellular ATP and other nucleotides and nucleosides (*e.g.* adenosine) exert these effects by activating a family of membrane bound receptors known as purinergic receptors or purinoceptors. Thus, purinergic signaling is implicated in various biological phenomenon including neurotransmission [2–4], inflammation [5], cell survival, motility as well as its proliferation, and differentiation [6]. All these ATP mediated responses are regulated by a cascade of enzymes known as ecto-nucleotidases. This enzymatic cascade is responsible for sequential hydrolysis of ATP to adenosine and comprises of four enzyme families including ecto-nucleoside triphosphate diphosphohydrolase (E-NTPDase), alkaline phosphatase (AP), ecto-nucleotide pyrophosphatase/phosphodiesterase (E-NPP), and ecto-5′-nucleotidase (eN) [7].

E-NTPDases represent a predominant family of eukaryotic enzymes characterized by the presence of five conserved domains known as “apyrase conserved region”. These domains consist of small stretches of amino acids containing residues which are vital for the proper functioning of enzyme. Moreover, enzyme activity also strictly depends on

* Corresponding authors.
E-mail addresses: drjamshed@cuiatd.edu.pk (J. Iqbal), ahassan@qau.edu.pk (A. Hassan).

https://doi.org/10.1016/j.bioorg.2019.03.019
Received 28 December 2018; Received in revised form 21 February 2019; Accepted 9 March 2019
Available online 12 March 2019
0045-2068/

the presence of divalent cations such as calcium and magnesium [8]. In mammals, E-NTPDases consist of eight members and they are named as NTPDase1-8. These enzymes have varying preference for nucleotides. NTPDase1, 3 and 8 hydrolyze nucleoside tri and diphosphate at an equal rate whereas NTPDase2 strongly prefers nucleoside triphosphate [9]. NTPDase1-3 and 8 are membrane bound proteins with an extracellular catalytic site. Although NTPDases4-7 have been associated with the intracellular organelles and membranes, secreted forms of NTPDase5 and NTPDase6 have also been identified. On the other hand, NTPDase4 and 7 are located within the organelles [8].

NTPDases are ubiquitously distributed in almost every tissue where they have been associated with various biological processes. However, they are over-expressed under certain pathological conditions *e.g.* in cancer and thus represent key drug targets for regulating the purinergic receptors mediated signaling pathways [10]. Therefore, to evaluate the (patho) physiological roles of NTPDases, there is a dire need to identify the selective and potent inhibitors of NTPDases. Moreover, such compounds can also be utilized for the treatment of various diseases such as cancer, cardiovascular, immunological, and CNS disorders.

Currently, only few classes of NTPDase inhibitor have been identified. They incorporate ATP analogs (ARL 67156), suramin, sulfonate dyes (reactive blue 2, PSB 069, PSB 06126), pyridoxal phosphate-6-azophenyl-2′,4′-disulfonic acid (PPADS) and polyoxometalates. However, all the above-mentioned compounds are non-selective in nature, except PSB 06126 that is specific inhibitor of NTPDase3 [11]. Moreover, our group has recently reported the Schiff bases of tyramine as potent inhibitors of NTPDases [12] (Fig. 1).

Quinoline scaffold is a versatile building block that has been found to be associated with natural products [13] as well as synthetic compounds [14,15]. They possess various biological effects; especially 2-arylquinolines have been reported to have anti-cancer [16], antimicrobial and anti-malarial effects [17]. Numerous strategies have been designed for the synthesis of quinoline derivatives *e.g.* Skraup [18], Riehm [19], Conrad-Limpach [20–22], Combes [23,24], Doebner-von Miller [25–27], and Pfitzinger [28,29] syntheses. Despite holding certain benefits these methods have been identified to have some problems including harsh reaction conditions, long reaction time, functional group intolerance and the use of promoters. On the other hand, there has been surge in the use of iodine as catalyst in organic synthesis [30,31], especially in heterocycle synthesis [32]. This iodine catalysis has also been utilized for quinoline synthesis through the Freidlander reaction using *o*-aminoacetophenone and activated ketones [33]. For instance a study reported the synthesis of quinolines by utilizing only 1 mol% molecular iodine as catalyst [34]. Similarly, another study described the synthesis of 2-arylbenzoquinoline by using 10 mol% iodine as the catalyst [35]. In accordance with the surging interest in iodine catalyzed heterocycle synthesis and our continuous quest to develop potent inhibitors of NTPDase [12], we have successfully synthesized a new series of quinoline derivatives as potential inhibitors of NTPDases.

2. Results and discussion

With the success of the molecular iodine catalyzed synthesis of quinoline derivatives, we wished to introduce hydroxyl substituted aliphatic aldehyde for induction of the aliphatic chain on the quinoline. In our hands, all efforts towards a three-component reaction of aniline, aromatic aldehydes and benzyloxy substituted aliphatic aldehydes failed to result in quinoline derivatives. In addition, a two-component reaction of arylimine and 2-benzyloxyacetaldehyde or 3-benzyloxypropionaldehyde did not result in any product, presumably due to side reactions of the activated aliphatic aldehyde.

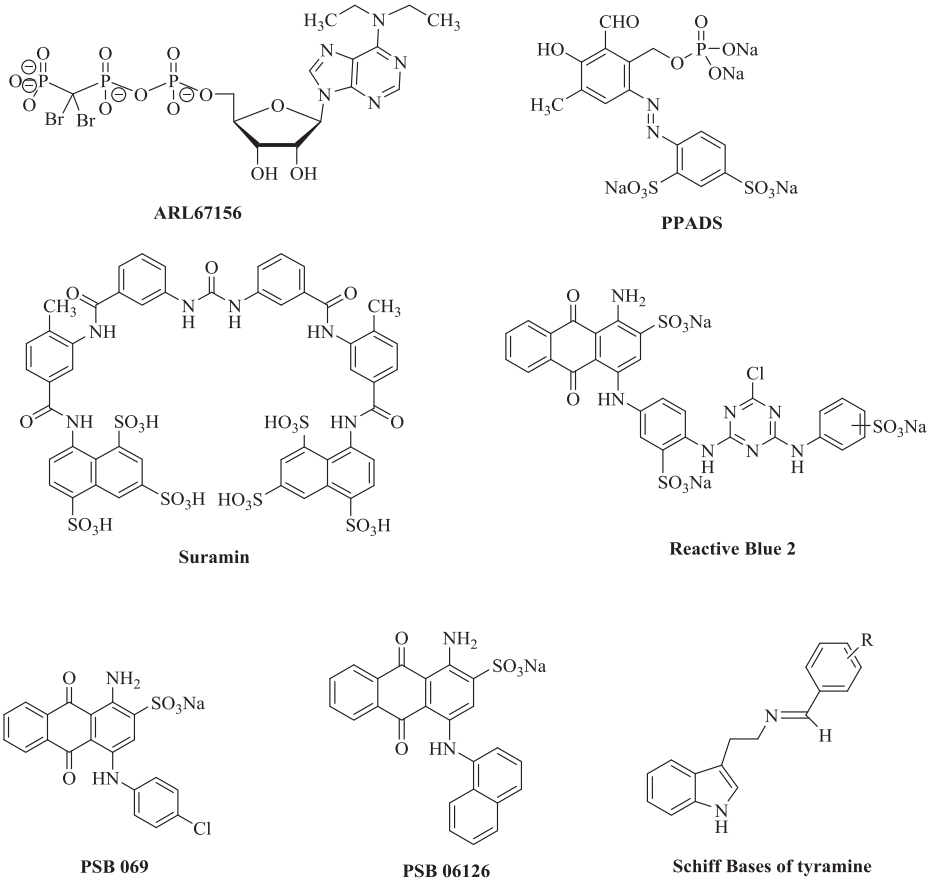

Fig. 1. Known inhibitors of NTPDases.

Table 1
Reaction optimization for arylimine and 5-benzyoxypentanal cyclization to quinolines

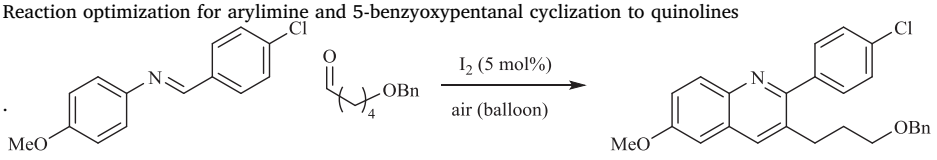

1b **2** **3o**

Entry	Solvent	Temp. (°C)	Time (h)	Yield (%)[a]
1	THF	60	16	15
2	THF	50	5	84
3	CH_3CN	50	5	61
4	DCE	50	5	66
5	DMSO	40	5	72
6	**DMSO**	**50**	**5**	**89**
7	DMSO	60	5	89

Reactions were performed using imine (0.5 mmol), 5-benzyloxypantanal (0.6 mmol) and iodine (0.025 mmol, 5 mol%) in (0.3 M) of solvent concentration under an air atmosphere.
[a] Isolated yields.

When 5-benzyloxypentanal **2** was treated with (*E*)-1-(4-chlorophenyl)-*N*-(4-methoxyphenyl)methanimine **1b** at 40 °C in dry THF as solvent in an open flask, it resulted in inseparable mixture of cyclized dihydroquinoline and quinoline products. It was inferred from the reaction mixture that 5-benzyloxypentanal consumes in reaction presumably through self-oxidation. Reproducible results were obtained when the reaction was carried out under air balloon and with the use of dry solvent. A quick screening of reaction solvent and temperature was performed. At 50 °C for 5 h, the quinoline was isolated in 84% yield (Table 1, entry 2). While when acetonitrile and dichloroethane was used as the solvent the yield drops considerably to 61% and 66%, respectively. Dimethyl sulfoxide (DMSO) was proved to be a superior solvent with isolated yield of product **3o** in 89% yield (Table 1, entry 6). Increasing or decreasing the temperature did not improve the yield (Table 1, entries 5 and 7). Similarly, increasing the iodine loading did not improve the yield.

With the optimized condition in hand the reaction was performed with different aldehydes and imine derivatives to synthesize diversely substituted quinoline derivatives **3a-3w**. Fortuitously, the optimized reaction condition was applicable to a variety of substrate. The arylimine **1a** resulted in the quinoline derivative **3a** in 53% yield after reaction with propionaldehyde. While using imine **1b**, derived from electron rich anisidine and electron poor 4-chlorobenzaldehyde after treating with propionaldehyde, resulted in product **3b** in 78% yield. The same imine **1b** was treated with variety of aliphatic aldehyde including butyraldehyde, valeraldehyde and octanal resulted in alkyl substituted quinolines **3c-e** in fair yields.

When (*E*)-*N*,1-diphenylmethanimine **1f** was treated with aldehyde **2** under the optimized reaction condition the quinoline **3f** was obtained in 58% yield. However, when the reaction was carried out at 60 °C it slightly improved the yield to 63%. The rest of quinolines were synthesized using aldehyde **2**. Similarly, when halogen substituted arylimines **1g** and **1h** were subjected to optimized reaction conditions the product **3g** and **3h** were obtained in 59% and 60% yield respectively. On the contrary methyl substituted imine **1i** derived from toluidine resulted in the product **3i** in 70% isolated yield. The higher yields in the case **3i** can be attributed to the electron releasing nature of the methyl group present on phenyl residue. In comparison with **1g** and **1h**, although halogens are *o*-, *p*-directing group, they diminish the electron donating capacity of aromatic ring due to their electron withdrawing nature (Table 2).

Interestingly, electron releasing substituent at R^2 position of imine provided diminished yields, as can be seen in the case of **3j** isolated in only 59%. In contrast, electron withdrawing group present at the 4-benzylidene position, derived from the aldehyde part of arylimine favored the reaction. Consequently, bromo substitution at R^2 resulted in the product **3k** in much higher yield (80%). The same trend persisted with chloro in the synthesis of **3l** which was isolated in 89% yield, however, the reaction required 9 h for its completion. When 4-nitrobenzaldehyde derived arylimines **1m** were subjected to iodine catalyzed optimized conditions the reaction should have been slow, however, the quinolines **3m** was isolated in 68% yield. All imines having methoxy group at position R^1 resulted in the corresponding products **3n-3p** in much higher yields. Similarly, various halogen substituted quinolines **3q-3w** were synthesized in good to moderate yields (Table 2).

As suggested previously [33], we can speculate the mild Lewis acid role for the iodine. The enol form of **2** undergoes addition to iodine activated imine resulting in first C—C bond formation. This enol imine alkylation results in the *β*-aminoaldehyde intermediate **4**. The presence of the EWG on imine derived from aldehyde counterpart lowers the LUMO of the imine, facilitating the reaction. Substituted arylimines having functional groups like MeO, Me and Br at aniline counterpart smoothly undergo cyclization reaction with 5-benzyloxypantanal to afford respective 2-aryl substituted quinoline derivatives. This attributed to the electron releasing nature of the substitution which decreases the HOMO-LUMO energy difference. Hence, the tethered electrophile will be easily cyclized to dihydroquinolines which upon air oxidation gave quinolines (Scheme 1). Apart from easy access to the quinolines these substitutions also provide diversity as well as a potential for further transformation.

2.1. Inhibition of NTPDase-1, -2, -3, and -8

2.1.1. Structure-activity relationship (SAR)

In the quest of finding the potent and selective inhibitors of human NTPDases, we analyzed current series of quinoline derivatives (Table 3). Most of the compounds inhibited either *h*-NTPDase1 and/or 8 with smaller effects on *h*-NTPDase2 and 3. Two compounds *i.e.* **3f** (IC_{50} = 13.9 ± 0.06 μM) and **3t** (IC_{50} = 29.3 ± 0.72 μM) were identified as selective inhibitors of *h*-NTPDase1, whereas **3s** (IC_{50} = 8.99 ± 0.67 μM) inhibited the *h*-NTPDase8 selectively, when compared with the standard suramin having IC_{50} values 16.1 ± 1.08 and 101.1 ± 2.34 μM, respectively.

Table 2
Synthesis of structurally diverse quinoline derivatives through iodine catalysis.

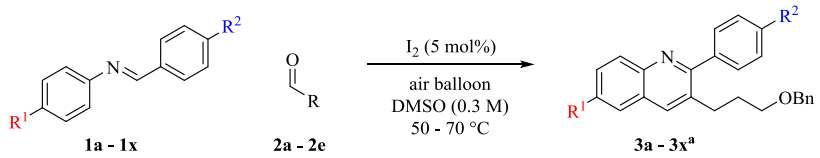

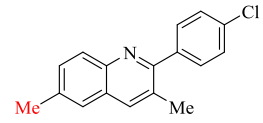

3a, 53%

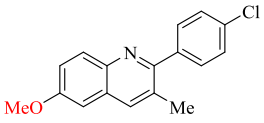

3b, 78%

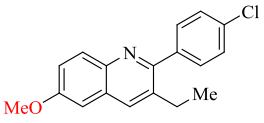

3c, 51%

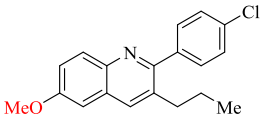

3d, 61%

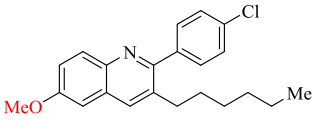

3e, 47%

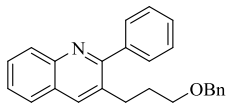

3f, 63%[b]

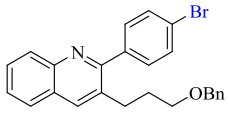

3g, 59%[b]

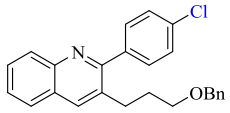

3h, 60%

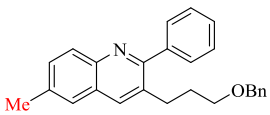

3i, 70%[b]

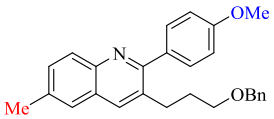

3j, 59%[b]

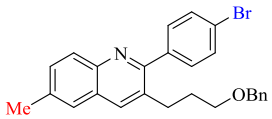

3k, 80%

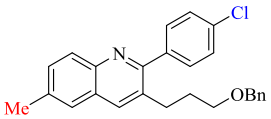

3l, 89%

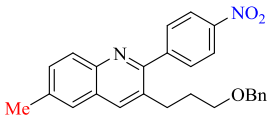

3m, 68%

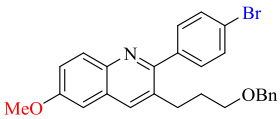

3n, 86%

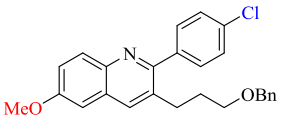

3o, 89%

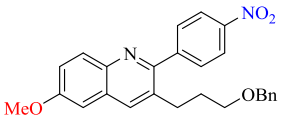

3p, 91%

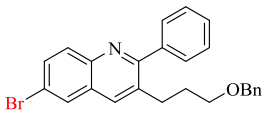

3q, 58%[b]

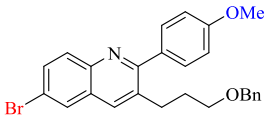

3r, 49%

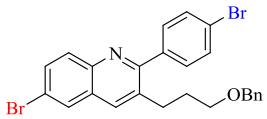

3s, 60%

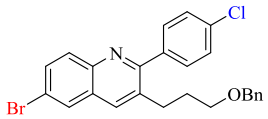

3t, 71%

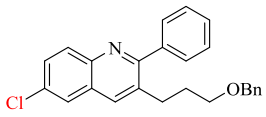

3u, 49%

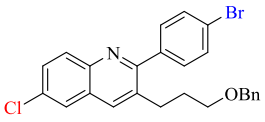

3v, 50%

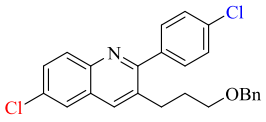

3w, 47%

All reactions were performed using imine (0.5 mmol), 5-benzyloxypantanal (0.6 mmol) and iodine (0.025 mmol, 5 mol %) in DMSO (0.3 M) under an air atmosphere at 50 °C. Isolated yields. [b]Reaction was performed at 60 °C. [c]Reaction was performed at 70 °C.

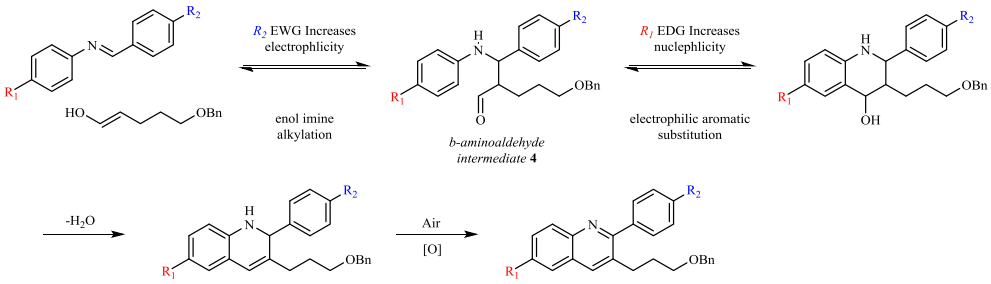

Scheme 1. Electronic nature of the arylimine dependent synthesis of quinoline.

Table 3
Nucleoside tri-phosphate diphosphohydrolases (NTPDase1, 2, 3 and 8) inhibitory activities of compounds (**3a-3w**).

Compound	*h*-NTPDase1	*h*-NTPDase2	*h*-NTPDase3	*h*-NTPDase8
	IC_{50} (μM)[a] ± SEM/%inhibition[b]			
3a	1.97 ± 0.05[a]	19.3 ± 0.09[b]	22.3 ± 0.11[a]	12.9 ± 0.22 [a]
3b	2.76 ± 0.02[a]	34.7 ± 0.16[b]	22.5 ± 1.06[a]	45.8 ± 0.43[a]
3c	2.77 ± 0.04[a]	22.8 ± 0.08[b]	12.5 ± 0.53[a]	1.13 ± 0.04[a]
3d	3.15 ± 0.10[a]	20.0 ± 0.1 [b]	5.38 ± 0.21[a]	65.6 ± 0.56[a]
3e	19.3 ± 0.11[a]	55.1 ± 0.02[a]	18.4 ± 0.12[a]	6.27 ± 0.11[a]
3f	13.9 ± 0.06[a]	21.7 ± 1.02[b]	5.97 ± 0.19[b]	45.1 ± 1.32[b]
3g	18.7 ± 0.45[a]	25.6 ± 0.23[b]	20.1 ± 0.09[b]	1.64 ± 0.07[a]
3h	32.5 ± 0.02[b]	26.1 ± 0.17[b]	14.3 ± 0.65[b]	38.8 ± 0.94[b]
3i	13.1 ± 0.02[a]	37.7 ± 0.27[b]	24.3 ± 0.33[b]	245.0 ± 1.05[a]
3j	1.04 ± 0.03[a]	21.0 ± 0.03[a]	8.19 ± 0.27[b]	18.3 ± 0.86[a]
3k	2.12 ± 0.08[a]	32.8 ± 0.15[b]	25.3 ± 0.78[b]	2.03 ± 0.05[a]
3l	6.06 ± 0.36[a]	22.5 ± 0.05[b]	35.9 ± 0.94[b]	28.6 ± 0.45[a]
3m	101.0 ± 1.23[a]	23.1 ± 0.13[b]	21.9 ± 0.56[b]	40.1 ± 0.89[a]
3n	21.2 ± 2.16[b]	28.5 ± 1.21[b]	2.52 ± 0.11[b]	27.1 ± 0.66[b]
3o	30.3 ± 0.28[b]	22.5 ± 0.55[b]	17.4 ± 0.71[b]	20.2 ± 0.36[b]
3p	0.23 ± 0.01[a]	34.1 ± 0.32[b]	37.0 ± 1.21[b]	8.44 ± 0.14[a]
3q	53.9 ± 0.67[a]	19.4 ± 0.14[b]	22.6 ± 0.77[b]	12.3 ± 0.87[a]
3r	30.2 ± 0.87[b]	27.5 ± 0.27[b]	4.87 ± 0.14[b]	32.1 ± 0.18[b]
3s	34.1 ± 1.08[b]	29.8 ± 0.19[b]	13.1 ± 0.51[b]	8.99 ± 0.67[a]
3t	29.3 ± 0.72[a]	31.3 ± 1.21[b]	18.5 ± 0.85[b]	45.1 ± 0.67[b]
3u	15.0 ± 0.46[b]	42.5 ± 0.98[b]	8.13 ± 0.38[b]	25.6 ± 0.64[b]
3v	10.1 ± 0.24[a]	36.3 ± 0.26[b]	27.6 ± 0.23[b]	3.11 ± 0.08[a]
3w	25.7 ± 0.88[a]	20.6 ± 0.11[b]	14.1 ± 0.21[b]	3.42 ± 0.12[a]
Suramin	16.1 ± 1.08[a]	24.1 ± 0.15 [a]	4.30 ± 0.84[a]	101.1 ± 2.34[a]

[a] IC_{50} values.
[b] % inhibition.

Among all the twenty-three compounds, seventeen compounds inhibited the *h*-NTPDase1 to a variable extent as reflected by their IC_{50} values (ranging from 0.23 ± 0.01 to 101.0 ± 1.23 μM), whereas suramin was used as the standard having an IC_{50} value of 16.1 ± 1.08 μM. These synthetic derivatives contained either an alkyl or bezyloxypropyl group as a part of quinoline ring. Those compounds containing an alkyl group (**3a-3e**) exhibited good to moderate inhibitory activity with an IC_{50} values ranging from 1.97 ± 0.05 to 19.3 ± 0.11 μM. The compound **3a** (IC_{50} = 1.97 ± 0.05 μM) having a simple methyl group was identified as a potent inhibitor of *h*-NTPDase1. However, an increase in the length of this alkyl chain led to a decreased activity. Among those compounds bearing a benzyloxylpropyl group, compound **3p** (IC_{50} = 0.23 ± 0.01 μM) was found to be the most potent inhibitor of *h*-NTPDase1 in the series. A detailed structure-activity relationship revealed that this derivative had NO_2 group at R^2 and an OCH_3 group at R^1 position. Although OCH_3 group is assumed to be electron donating but here it could be suggested to withdraw the electrons inductively. Whereas NO_2 group present at R^2 is already electron withdrawing. Thus, the enhanced inhibitory activity of **3p** may be attributed to this combination of two electron withdrawing groups, since replacement of this OCH_3 group with an electron donating group *i.e.* CH_3 (**3m**) lead to the least potent inhibitor of *h*-NTPDase1. The compound **3m** exhibited ~439 times less activity as compared to the most potent inhibitor **3p**, of *h*-NTPDase1. Moreover, it can also be suggested that this OCH_3 group is best suited with NO_2 group since OCH_3 group in combination with any halogen atom **3n**, **3o**, and **3r** did not show considerable inhibition of *h*-NTPDase1. Likewise, the next compound **3j** (IC_{50} = 1.04 ± 0.03 μM) showing the good inhibitory activity towards *h*-NTPDase1 also had an OCH_3 group at R^2 position thus emphasizing the importance of OCH_3 group. Moreover, the introduction of methyl group at R^1 also led to good inhibitory activity against *h*-NTPDase1 as presented by the IC_{50} values of the compounds **3i** (IC_{50} = 13.1 ± 0.02 μM), **3k** (IC_{50} = 2.12 ± 0.08 μM), and **3l** (IC_{50} = 6.06 ± 0.36 μM).

Another important factor affecting the inhibitory activity of compounds was position of substituent. A comparison of R^1 and R^2 position showed that R^1 position was more suitable for electron donating groups like CH_3, OCH_3 whereas the electron withdrawing groups preferred the R^2 position. For instance, **3g** (IC_{50} = 18.7 ± 0.45 μM) having Br at R^2 and **3i** (IC_{50} = 13.1 ± 0.02 μM) with CH_3 group at R^1 showed considerable activity. Combination of these two groups in **3k** (IC_{50} = 2.12 ± 0.08 μM) resulted in exceedingly high biological activity (see Fig. 2).

Likewise, the presence of Br at R^2 imparted greater activity to **3g** (IC_{50} = 18.7 ± 0.45 μM) as compared to **3q** (IC_{50} = 53.9 ± 0.67 μM) where Br is present at R^1. Another example is **3r** where R^1 position was occupied by electron withdrawing group (Br) whereas R^2 position contained an electron donating group (OCH_3) and the resulting derivative was inactive towards *h*-NTPDase1. However, the compound **3j** (IC_{50} = 1.04 ± 0.03 μM), containing electron donating group at both R^1 and R^2 position, was an exception. It is suggested that the OCH_3 group is operating by negative inductive effect and thus acting as electron withdrawing group. Other exceptions are **3n** and **3o** where R^1 positions are equipped with electron donating group whereas R^2 positions have electron withdrawing groups. Though, it is already explained that OCH_3 group is best suited with NO_2 group. It is noteworthy that CH_3 group was well tolerated with halogens and showed good inhibitory activity. It can be exemplified by the inhibitory activity of **3k** (IC_{50} = 2.12 ± 0.08 μM) and **3l** (IC_{50} = 6.06 ± 0.36 μM).

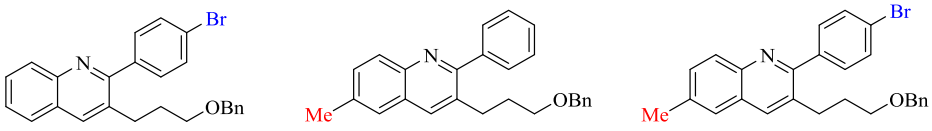

3g IC_{50} = 18.7 ± 1.54 μM

3i IC_{50} = 13.1 ± 1.23 μM

3k IC_{50} = 2.12 ± 0.36 μM

Fig. 2. The enhanced combination effect of substitution (**3k**) for the inhibition of *h*-NTPDase1.

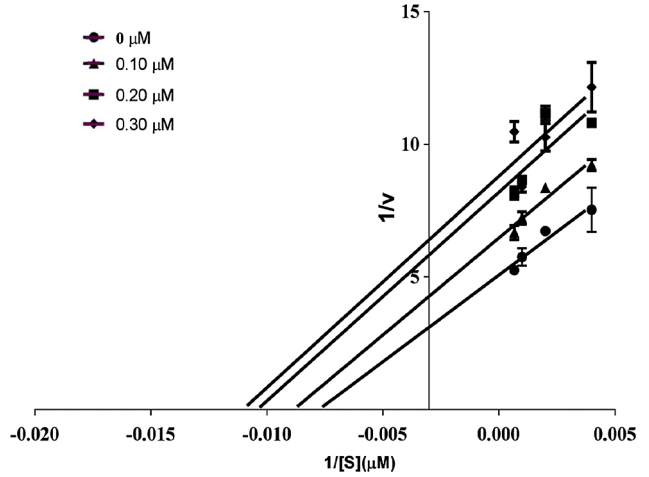

Fig. 3. Lineweaver-Burk Plot of compound **3p** agianst *h*-NTPDase1. S: is the concentration of substrate used (μM); concentration of compound **3p** black circle, 0 μM; black triangle, 0.1 μM; black square, 0.2 μM; and black diamond, 0.3 μM.

Comparison of the same derivatives *i.e.* **3k** and **3l** showed that derivatives bearing Br at R^2 were more active than those with Cl. It was further emphasized by the comparison of **3t** (IC_{50} = 29.3 ± 0.72 μM) and **3v** (IC_{50} = 10.1 ± 0.24 μM).

All compounds showed less inhibitory potential *i.e.* less than 50% inhibition against *h*-NTPDase2 except **3e** and **3j**. The compound **3j** having an IC_{50} value of 21.0 ± 0.03 μM was comparable to that of suramin (24.1 ± 0.15 μM), however, the compound **3e** (IC_{50} = 55.1 ± 0.02 μM) was much less active as compared to suramin.

In case of *h*-NTPDase3, compounds having alkyl group as substituents attached to quinoline ring could inhibit the enzyme. Moreover, the IC_{50} values of these compounds suggested that inhibitory activity was affected by the length of alkyl chain. The compounds containing ethyl, propyl or hexyl group exhibited good inhibitory activity i-e., **3c** (IC_{50} = 12.5 ± 0.53 μM), **3d,** (IC_{50} = 5.38 ± 0.21 μM), and **3e** (IC_{50} = 18.4 ± 0.12 μM) as compared to those having methyl group **3a** (IC_{50} = 22.3 ± 0.11 μM) and **3b** (IC_{50} = 22.5 ± 1.06 μM). However, none of them was more active than the standard suramin (IC_{50} = 4.30 ± 0.84 μM). Thus, the activity of these compounds might be attributed to the presence of alkyl chain attached to quinoline ring since the incorporation of benzyloxy at the end of propyl group resulted in the loss of activity (**3f-3w**).

Most of the compounds were identified as dual inhibitors of *h*-NTPDase1 and 8. This was especially found to be true for compounds **3a-3e**. Among these compounds, **3c** (IC_{50} = 1.13 ± 0.04 μM) was recognized as the most potent inhibitor of *h*-NTPDase8. Activity of this compound might be attributed to the presence of ethyl group attached to quinoline ring since any variation in this group resulted in reduced activity. However, selectivity was also identified among benzyloxypropyl substituted derivatives (**3f-3w**). For example, compound **3f** and **3t** selectively inhibited *h*-NTPDase1, whereas compound **3s** (IC_{50} = 8.99 ± 0.67 μM) was found to be the selective inhibitor of *h*-NTPDase8. Moreover, parent compound of these derivatives (**3f-3w**) *i.e.* **3f** did not show considerable activity towards *h*-NTPDase8. However, certain modifications at R^1/R^2 led to significant inhibitory potential. In this regard, compounds containing Br at R^2 exhibited excellent inhibitory activity. For example, compound **3g** (bearing Br at R^2 position) displayed the highest inhibitory activity with an IC_{50} value of 1.64 ± 0.07 μM that is ~65 times higher than the standard suramin (IC_{50} = 101.1 ± 2.34 μM). However, introduction of an electron donating group *i.e.* CH_3 group at R^1 position in **3k** (IC_{50} = 2.03 ± 0.05 μM) led to slight reduction in inhibitory activity. Likewise, introduction of electron withdrawing group *i.e.* Cl at R^1 (**3v**) further reduced the activity (IC_{50} = 3.11 ± 0.08 μM) towards *h*-NTPDase8. There were some other modifications that sufficiently affected the inhibitory activity of synthetic analogs. For example, a comparison between IC_{50} values of **3m** and **3p** revealed that replacement of methyl group (**3m**) with methoxy (**3p**) improved the inhibitory activity by ~5 times. Similarly, modification in position of substituent also played an important role as it could be exemplified by comparing the IC_{50} values of **3q** (12.3 ± 0.87 μM) and **3g** (1.64 ± 0.07 μM). In this case, placement of Br at R^2 (**3g**) instead of R^1 (**3q**) resulted in an IC_{50} value that was ~12 times high as compared to that of **3g**.

Some patterns of structure-activity relationship observed for *h*-NTPDase1 were also consistent with *h*-NTPDase8. For instance, the electron donating groups preferred R^2 position as compared to R^1 and it is observed by comparing the IC_{50} values of **3g** (IC_{50} = 1.64 ± 0.07 μM) to that of **3q** (IC_{50} = 12.3 ± 0.87 μM). Yet again, presence of NO_2 group in combination with OCH_3 group appeared to be an important determinant of inhibitory activity since the compound **3p** (IC_{50} = 8.44 ± 0.14 μM) possessed ~5 and ~8 folds more inhibitory activity as compared to **3m** (IC_{50} = 40.1 ± 0.89 μM) and **3t** (IC_{50} = 45.1 ± 0.67 μM). Another pattern observed was related to Br. Here again, presence of Br at R^1 resulted in reduced activity as seen in case of **3q** (IC_{50} = 12.3 ± 0.87 μM) and **3s** (IC_{50} = 8.99 ± 0.67 μM) and eventually lead to loss of activity as exemplified by **3t** (IC_{50} = 45.1 ± 0.67 μM).

However, varying behavior was also observed while deriving the structure-activity relationship for *h*-NTPDase8. In this context, most important point was related to compounds substituted with electron donating groups. Here such compounds possessed much less inhibitory activity and it was reflected by the IC_{50} value of **3i** (IC_{50} = 245.0 ± 1.05 μM). However, when the R^2 position was replaced by electron withdrawing groups such as Br **3k** (IC_{50} = 2.03 ± 0.05 μM) and Cl **3l** (IC_{50} = 28.6 ± 0.45 μM), an improvement in inhibitory activity was observed. Moreover, it is noteworthy that **3s** (IC_{50} = 8.99 ± 0.67 μM) was selective inhibitor of *h*-NTPDase8. Although the compound **3g** (IC_{50} = 1.64 ± 0.07 μM) having Br at R^2 showed good inhibitory activity for *h*-NTPDase1 which is an exception. The dibromo substitution in **3s** (IC_{50} = 8.99 ± 0.67 μM) resulted in selective inhibition of *h*-NTPDase8.

In view of above discussion, it can be concluded that the nature and position of substituents significantly affected the inhibitory potential of

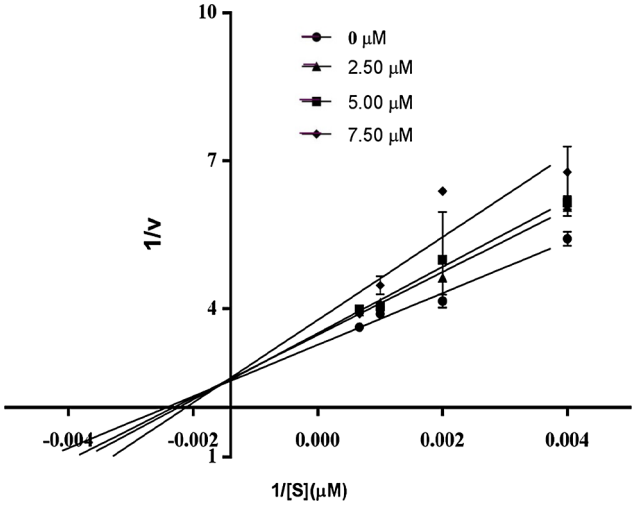

Fig. 4. Lineweaver-Burk Plot of compound **3d** agianst *h*-NTPDase3. S: is the concentration of substrate used (μM); concentration of compound **3d**, black circle, 0 μM; black triangle, 2.5 μM; black square, 5.0 μM; and black diamond, 7.5 μM.

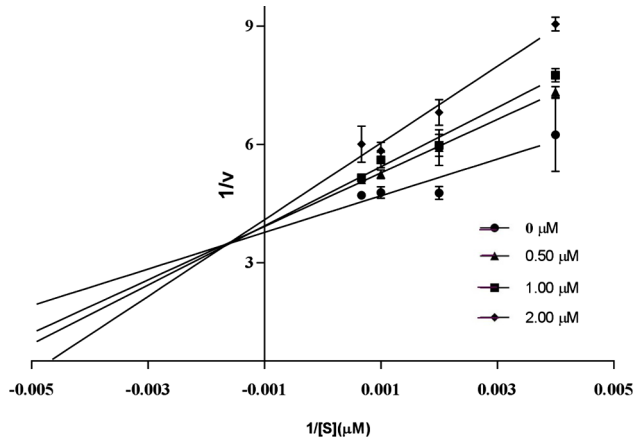

Fig. 5. Lineweaver-Burk Plot of compound **3c** agianst *h*-NTPDase8. S: is the concentration of substrate used (μM); concentration of compound **3c**, black circle, 0 μM; black triangle, 0.5 μM; black square, 1.0 μM; and black diamond, 2 μM.

these compounds against *h*-NTPDase1, 3 and 8.

2.1.2. Mechanism of inhibition

The most potent inhibitor of *h*-NTPDase1, 3 and 8 (**3p**, **3d** and **3c**, respectively) were selected to determine the mechanism of inhibition. The compound **3p** was identified as uncompetitive inhibitor of *h*-NTPDase1, whereas, the compounds **3d** and **3c** competitively inhibited the *h*-NTPDase3 and 8, respectively (Figs. 3–5).

2.2. Molecular docking studies

To justify the *in vitro* enzyme inhibition of NTPDases, docking studies were performed against NTPDase1, 3 and 8 modeled structures [36]. The experimental results suggested that compound **3p** was selective inhibitor of *h*-NTPDase1, compound **3d** and **3c** were potent inhibitors of *h*-NTPDase3 and *h*-NTPDase8, respectively. However, no compound was found selective or potent against *h*-NTPDase2, therefore, the docking studies were not carried out for *h*-NTPDase2.

2.3. NTPDase1 docking studies

Amino acid residues in the active site pocket of *h*-NTPDase1 are His59, Ser58, Gly56, Asp213, Ser361, Gly449 and Ca^{++} for compound **3p** (olive green) (3-(3-(benzyloxy)propyl)-6-methoxy-2-(4-nitrophenyl) quinoline). The hydrogen bond interactions were observed between the oxygen of benzyloxypropyl and Ser361 residue, furthermore the quinoline ring was involved in π-alkyl interactions with Asp213. However, the oxygen atom of 6-methoxy was involved in hydrogen bonding with the Gly449. The other hydrogen bonds formed by 4-nitrophenyl group were found with His59, Ser58 and Gly56. The metal interactions were noticed by calcium and 4-nitrophenyl ring, which indicate that the part of the compound **3p** was oriented towards the deep active site pocket of *h*-NTPDase1. The Ca^{++} is very important for the catalytic activity of NTPDase1. However, from Fig. 6 it was shown that quinoline part and benzyloxypropyl moiety was found towards the entrance of the active site, whereas, the 4-nitrophenyl ring was observed in the deep pocket towards the Calcium ion. The involvement of metal ion represented the uncompetitive selectivity of compound **3p** towards NTPDase1 (Fig. 6), as reported in the enzyme inhibition study.

2.4. NTPDase3 docking studies

In the active site of NTPDase3 (Fig. 7), compound **3d** (blue color) (2-(4-chlorophenyl)-6-methoxy-3-propylquinoline) was present in the deeper active pocket. The important residues Arg67, Ser66, Lys95 and

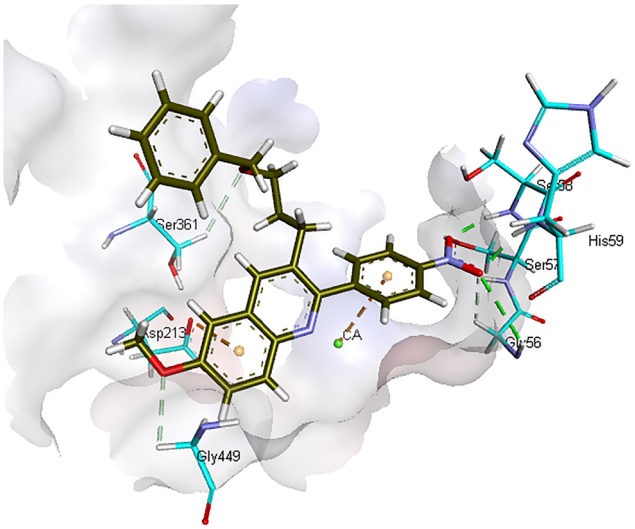

Fig. 6. Possible binding mode of **3p** (olive green color) in *h*-NTPDase1 active site (cyan color), the dashed lines represent Hydrogen and π bonds while as the sphere is Ca^{++} metal.

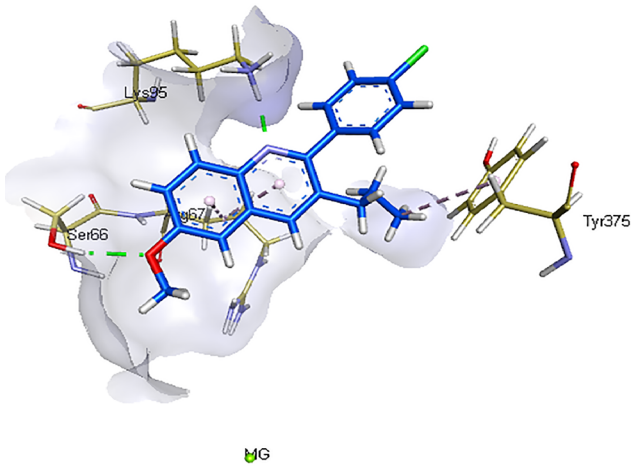

Fig. 7. Possible binding mode of **3d** (blue color) in *h*-NTPDase3 active site (olive green color), the dashed lines represents Hydrogen (green) and π bonds (pink) and the sphere shows Mg^{++} metal.

Tyr375 of NTPDase3 were involved in the interaction with compound **3d**. The nitrobenzene of quinoline nucleus was observed in hydrogen bonding with Lys95 and π-π stacked interactions with Arg67. Furthermore, the methoxy group was observed to be involved in hydrogen bonding with Ser66, while nitrogen atom of the quinoline ring was involved in hydrogen bonding with Lys95. Residue Tyr375 was in π–alkyl interactions with the propyl group. However, 4-chloro phenyl group was not found to involve in any interactions with the amino acid residues of the active site. Magnesium metal was observed in the catalytic region which is important for catalysis of NTPDase3 enzyme activity.

2.5. NTPDase8 docking studies

In the active site of NTPDase8 (Fig. 8), compound **3c** (green color) (2-(4-chlorophenyl)-3-ethyl-6-methoxyquinoline) was present in the profound position of binding pocket. The important residues His53, Tyr357, Arg249, Trp398 and Asp401 of NTPDase8 were involved in the interaction with compound **3c**. The quinoline ring was observed in making π-π stacked interactions with Trp398 as the amino acid was found parallel to the quinoline ring of the compound **3c**. However,

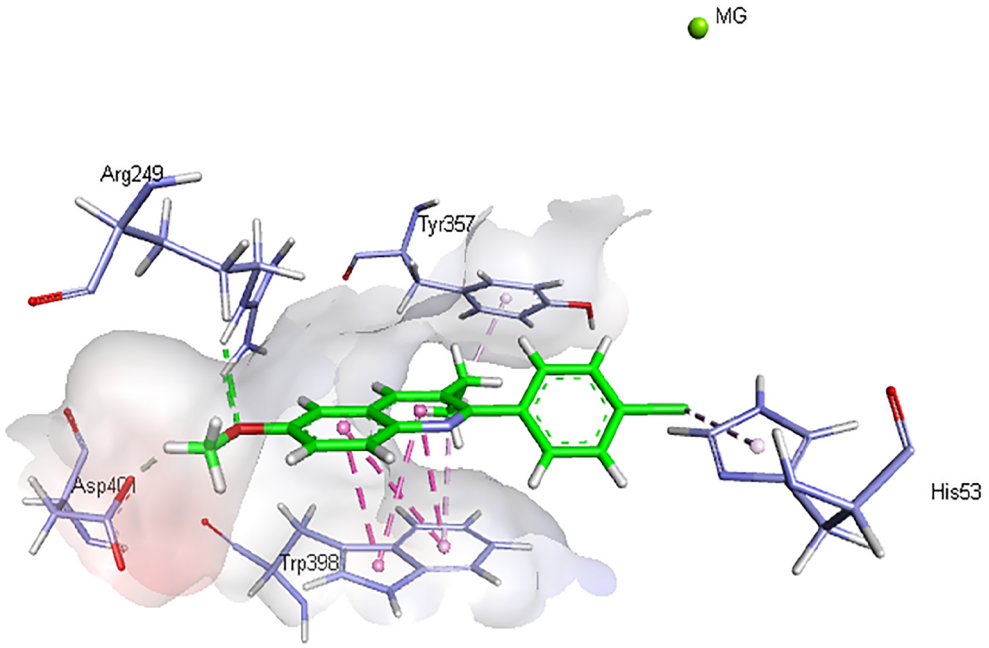

Fig. 8. Possible binding mode of **3c** (green color) in NTPDase8 active site (pink color), the dashed lines represents Hydrogen (green) and π bonds (pink) and the sphere shows Mg^{++} metal.

carbon-H bond was noticed between 6-methoxy and Asp401 residue. Halogen-π interactions were found between 4-chlorophenyl ring and imidazole ring of His53. In addition, two hydrogen bonds were formed by oxygen atom of 6-methoxy moiety and Arg249. Magnesium metal was also observed in the catalytic region which is important for catalysis of NTPDase8 enzyme activity. Therefore, the interaction pose of compound **3c** in the active pocket of NTPDase8 supported the *in vitro* enzyme competitive inhibition pattern of selectivity.

3. Conclusion

A mild and efficient iodine catalyzed quinoline synthesis has been applied for the synthesis of 3-benzyloxypropyl substituted highly functionalized 2-arylquinoline derivatives. The method used molecular iodine (I_2) as catalyst. Arylimines (**1a–1w**) obtained from aromatic aldehydes and anilines were cyclized with aliphatic aldehyde including 5-benzyloxypantanal (**2**) resulting in arylquinoline derivatives in appreciable yield. The reaction efficiency was contingent with the electronic nature of substitutions. The arylimines derived from aniline having EDG and aldehydes having EWG were found to be better substrate for the quinoline synthesis. The product conversion agrees to the proposed reaction mechanism. The functionalized quinoline derivatives (**3a–3w**) have the potential for further elaboration to more complex products. These quinoline derivatives (**3a-3w**) were evaluated as inhibitors of *h*-NTPDase1, 2, 3 and 8. Most of the compounds were able to inhibit *h*-NTPDase1 and/or *h*-NTPDase8. Although *h*-NTPDase3 remained resistant to most of the compounds, only five compounds could inhibit this enzyme. Excellent inhibitory activity was exhibited by the compound **3p** that inhibited the *h*-NTPDase1 with an IC_{50} value of 0.23 ± 0.01 μM (70 folds higher than the standard suramin). Moreover, two compounds *i.e.* **3f** and **3t** were identified as the selective inhibitor of *h*-NTPDase1. Likewise, **3c** was found to be the most potent inhibitor of *h*-NTPDase8 with an IC_{50} value of 1.13 ± 0.04 μM. In addition, the compound **3s** selectively inhibited the *h*-NTPDase8. In order to rationalize the binding interactions, molecular docking studies were also conducted.

4. Experimental

Detail experimental condition for the synthesis of compounds **3a-3w** and analytical data including, ^{1}H NMR, ^{13}C NMR, HRMS and FTIR and selected ^{1}H NMR and ^{13}C NMR spectra are given in the supporting information file.

4.1. General procedure for the synthesis of quinoline *3a-3w*

To a 25 mL round-bottomed flask was added arylimine (0.5 mmol, 100 mol%), molecular iodine (0.025 mmol, 5 mol%) in DMSO (1.7 mL, 0.3 M) and 5-benzyloxypantanal (0.6 mmol, 120 mol%). The round-bottomed flask was fitted with rubber septum and air balloon (the balloon was filled from air pump passing through dry magnesium sulfate). The reaction mixture was stirred at 50 °C for 5 h, monitored by TLC and confirmed by PMA-stain. After 5 h, water (20 mL) was added to the reaction mixture. The reaction mixture was extracted with ethyl acetate (30 mL × 3). The combined organic layer was concentrated *in vacuo* and purified by flash column chromatography (ethyl acetate: *n*-hexane, 1:10).

4.2. Bioassay protocols

Cell Transfection with Human NTPDase: The plasmids expressing human NTPDases *i.e.* *h*-NTPDase1 [37], *h*-NTPDase2 [38], *h*-NTPDase3 [39] and *h*-NTPDase8 [40] were transfected with COS-7 in 10-cm plates using Lipofectamine, as previously reported [41]. The confluent cells (80–90%) were incubated at 37 °C for 5 h, in Dulbecco's modified Eagle's medium (DMEM) (in the absence of fetal bovine serum (FBS)) with 24 μL of Lipofectamine reagent and 6 μg of plasmid DNA. Finally, transfection was stopped by adding same volume of DMEM/F-12 containing 20% FBS and cells were harvested 40–72 h later.

4.3. Preparation of membrane fractions

After transfection, the cells were washed with Tris-saline buffer at 4 °C. Subsequently, cells were collected by scraping in the harvesting buffer (95 mM NaCl, 0.1 mM PMSF and 45 mM Tris at pH 7.5) and again washed by centrifugation at 300*g* for 5 min (4 °C) [39]. The cells

acquired by centrifugation were re-suspended in the harvesting buffer carrying aprotinin (10 μg/μL) and then sonicated. Afterwards, cellular debris and nucleus were isolated by centrifugation at 4 °C for 10 min (300*g*). The resulting supernatant *i.e.* crude protein extract was aliquoted and stored at −80 °C until further use. In order to determine the protein concentration, Bradford microplate assay [42] was conducted whereas bovine serum albumin was used as a reference standard.

4.4. Nucleoside triphosphate diphosphohydrolase inhibition assay

The NTPDase inhibition assay was performed by previously reported method [43] with slight modification. The reaction buffer was composed of 50 mM Tris-HCl and 5 mM $CaCl_2$ (pH 7.4). The total assay volume of 100 μL contained 45 μL of Tris buffer, 10 μL of test compound (0.5 mM with final DMSO 1% (v/v)) and 10 μL of *h*-NTPDase1 (58 ng of protein/well) or *h*-NTPDase2 (165 ng of protein/well) or *h*-NTPDase3 (163 ng of protein/well) or *h*-NTPDase8 (66 ng of protein/well). The reaction mixture was incubated for 10 min at 37 °C for 10 min and the absorbance was measured at 630 nm as pre-read using microplate reader (BioTek ELx800 Instruments, Inc. USA Then 10 μL of substrate *i.e.* adenosine triphosphate (0.5 mM) was added to initiate the reaction and it was incubated for 20 min at 37 °C. Subsequently, 25 μL of malachite green reagent was added and change in absorbance was measured as after-read after 6–8 min. All experiments were carried out in triplicate. Compounds which exhibited over 50% inhibition of any isozyme of *h*-NTPDase activity were further evaluated for determination of IC_{50} values. Nonlinear curve fitting program PRISM 5.0 (GraphPad, San Diego, California, USA) was used for the determination of IC_{50} values.

4.5. Molecular docking studies of NTPDases

To understand the binding pattern of the most potent NTPDase1, 3 and 8 inhibitors, docking studies were performed using modeled structures [35]. The chemical structures of potent inhibitors were optimized in 3D using Marvin Sketch of Chem Axon suit [44]. After removal of water molecules, the energy of proteins was minimized and protonated in 3D using MOE (2014.009). (Molecular Operating Environment) software [45]. 50 confirmatory docked poses were generated using Affinity-dG feature of MOE with MMFF94X force field and the configurations with the lowest binding energies were selected and visualized using Discovery Studio Visualizer [46].

Acknowledgements

A. Hassan is grateful to Higher Education Commission, Pakistan for the financial support under the NRPU grant number 20-3069/NRPU/R &D/13. J. Iqbal is thankful to the Organization for the Prohibition of Chemical Weapons (OPCW), The Hague, The Netherlands and Higher Education Commission of Pakistan for the financial support through Project No. 20-3733/NRPU/R&D/14/520. J. Sévigny was supported by grants from the Canadian Institutes of Health Research. J.S. is also a recipient of a “Chercheur National” Scholarship award from the “Fonds de recherche du Québec-Santé” (FRQS).

Appendix A. Supplementary material

Supplementary data to this article can be found online at https://doi.org/10.1016/j.bioorg.2019.03.019.

References

[1] G.G. Yegutkin, Biochim. Biophys. Acta Mol. Cell Res. 1783 (5) (2008) 673–694.
[2] F.P. Gendron, E. Halbfinger, B. Fischer, M. Duval, P. D'Orléans-Juste, A.R.J. Beaudoin, Med. Chem. 43 (11) (2000) 2239–2247.
[3] N. White, G. Burnstock, Trends Pharmacol. Sci. 27 (4) (2006) 211–217.
[4] F. Di Virgilio, Cancer Res. 72 (21) (2012) 5441–5447.
[5] M.J. Bours, P.C. Dagnelie, A.L. Giuliani, A. Wesselius, F. Di Virgilio, Front. Biosci. (Schol Ed) 3 (2011) 1443–1456.
[6] J. Stagg, M.J. Smyth, Oncogene 29 (39) (2010) 5346.
[7] D. Brisevac, M. Adzic, D. Laketa, A. Parabucki, M. Milosevic, I. Lavrnja, I. Bjelobaba, J. Sévigny, M. Kipp, N. Nedeljkovic, J. Mol. Neurosci. 57 (3) (2015) 452–462.
[8] F.M. Sansom, Parasit. 139 (8) (2012) 963–980.
[9] J. Stella, L. Bavaresco, E. Braganhol, L. Rockenbach, P.F. Farias, M.R. Wink, A.A. Azambuja, C.H. Barrios, F.B. Morrone, A.M.O. Battastini, UROL Oncol-Semin Ori. 28 (3) (2010) 260–267.
[10] A. Fiene, Y. Baqi, J. Lecka, J. Sévigny, C.E. Müller, Analyst 140 (1) (2015) 140–148.
[11] Y. Baqi, S. Weyler, J. Iqbal, H. Zimmermann, C.E. Müller, Purinergic Signal. 5 (1) (2009) 91.
[12] K.M. Khan Kanwal, U. Salar, S. Afzal, A. Wadood, M. Taha, S Perveen, H. Khan, J. Lecka, J. Sévigny, J. Iqbal, Bioorg. Chem. 82 (2019) 253–266.
[13] G.A. Montalban, Quinolines and isoquinolines, in: K.C. Majumdar, S.K. Chattopadhyay (Eds.), Heterocycles in Natural Product Synthesis, 2011, pp. 299–339.
[14] V.R. Solomon, H. Lee, Curr. Med. Chem. 18 (10) (2011) 1488–1508.
[15] S. Kumar, S. Bawa, H. Gupta, Mini Rev. Med. Chem. 9 (14) (2009) 1648–1654.
[16] S. Jain, V. Chandra, P.K. Jain, K. Pathak, D. Pathak, A. Vaidya, Arab. J. Chem. (article in press) https://doi.org/10.1016/j.arabjc.2016.10.009.
[17] S. Bawa, S. Kumar, S. Drabu, R. Kumar, J. Pharm. Bioallied Sci. 2 (2) (2010) 64–71.
[18] R.H. Manske, M. Kulka, Org. React. 7 (1953) 80–99.
[19] Z. Riehm Wang, Quinoline synthesis, in: Z. Wang (Ed.), Comprehensive Organic Name Reactions and Reagents, John Wiley, 2010.
[20] R. Manske, Chem. Rev. 30 (1) (1942) 113–144.
[21] R.H. Reitsema, Chem. Rev. 43 (1) (1948) 43–68.
[22] M. Conrad, L. Limpach, Eur. J. Inorg. Chem. 20 (1) (1887) 944–948.
[23] A. Combes, Bull. Soc. Chim. France 49 (1883) 89.
[24] J.L. Born, J. Org. Chem. 37 (24) (1972) 3952–3953.
[25] O. Doebner, Eur. J. Inorg. Chem. 14 (2) (1881) 2812–2817.
[26] S.E. Denmark, S. Venkatraman, J. Org. Chem. 71 (4) (2006) 1668–1676.
[27] M. Heravi, S. Asadi, F. Azarakhshi, Curr. Org. Syn. 11 (5) (2014) 701–731.
[28] M.G.-A. Shvekhgeimer, Chem. Heterocycl. Compd. 40 (3) (2004) 257–294.
[29] N.P. Buu-Hoi, R. Royer, N.D. Xuong, P. Jacquignon, J. Org. Chem. 18 (9) (1953) 1209–1224.
[30] M. Jereb, D. Vražič, M. Zupan, Tetrahedron 67 (7) (2011) 1355–1387.
[31] Y.M. Ren, C. Cai, R.C. Yang, RSC Adv. 3 (20) (2013) 7182–7204.
[32] P.T. Parvatkar, P.S. Parameswaran, S.G. Tilve, Chem.A Eur. J. 18 (18) (2012) 5460–5489.
[33] M.A. Zolfigol, P. Salehi, A. Ghaderi, M. Shiri, J. Chin. Chem. Soc. 54 (2) (2007) 267–271.
[34] X.F. Lin, S.L. Cui, Y.G. Wang, Tetrahedronlett. 47 (18) (2006) 3127–3130.
[35] X.-S. Wang, Q. Li, J.R. Wu, Y.L. Li, Synth. Comm. 39 (4) (2009) 702–715.
[36] J. Iqbal, S.J.A. Shah, Sci. Rep. 8 (1) (2018) 2581.
[37] E. Kaczmarek, K. Koziak, J. Sévigny, J.B. Siegel, J. Anrather, A.R. Beaudoin, F.H. Bach, S.C. Robson, J. Biol. Chem. 271 (51) (1996) 33116–33122.
[38] S.M. Vlajkovic, G.D. Housley, D. Greenwood, P.R. Thorne, Evidence for alternative splicing of ecto-ATPase associated with termination of purinergic transmission, Brain Res. Mol. Brain Res. 73 (1999) 85–92.
[39] A.F. Knowles, W.C. Chiang, Arch. Biochem. Biophys. 418 (2) (2003) 217–227.
[40] T.M. Smith, T.L. Kirley, Biochim. Biophys. Acta 1386 (1) (1998) 65–78.
[41] F. Kukulski, S.A. Lévesque, E.G. Lavoie, J. Lecka, F. Bigonnesse, A.F. Knowles, S.C. Robson, T.L. Kirley, J. Sévigny, Purinergic Signal 1 (2) (2005) 193.
[42] M.M. Bradford, Anal. Biochem. 72 (1976) 248.
[43] J. Sévigny, C. Sundberg, N. Braun, O. Guckelberger, E. Csizmadia, I. Qawi, M. Imai, H. Zimmermann, S.C. Robson, Blood 99 (8) (2002) 2801.
[44] ChemAxon M, ChemAxon. Ltd., 2017.
[45] MOE (The Molecular Operating Environment) Version 2014.0901, Chemical Computing Group, (CCG) http://www.chemcomp.com/MOEMolecular_Operating_Environment.htm.
[46] Accelrys Software Inc., Discovery Studio Modeling Environment, Release 4.0, Accelrys Software Inc., San Diego, CA, 2013.